Science Advances
AAAS

Supplementary Materials for

2.4-Å structure of the double-ring *Gemmatimonas* phototrophica photosystem

Pu Qian*, Alastair T. Gardiner, Ivana Šímová, Katerina Naydenova, Tristan I. Croll, Philip J. Jackson, Nupur, Miroslav Kloz, Petra Čubáková, Marek Kuzma, Yonghui Zeng, Pablo Castro-Hartmann, Bart van Knippenberg, Kenneth N. Goldie, David Kaftan, Pavel Hrouzek, Jan Hájek, Jon Agirre, C. Alistair Siebert, David Bína, Kasim Sader, Henning Stahlberg, Roman Sobotka, Christopher J. Russo, Tomáš Polívka, C. Neil Hunter, Michal Koblížek*

*Corresponding author. Email: pu.qian@thermofisher.com (P.Q.); koblizek@alga.cz (M.Ko.)

Published 16 February 2022, *Sci. Adv.* **8**, eabk3139 (2022)
DOI: 10.1126/sciadv.abk3139

The PDF file includes:

Other Supplementary Material for this manuscript includes the following:

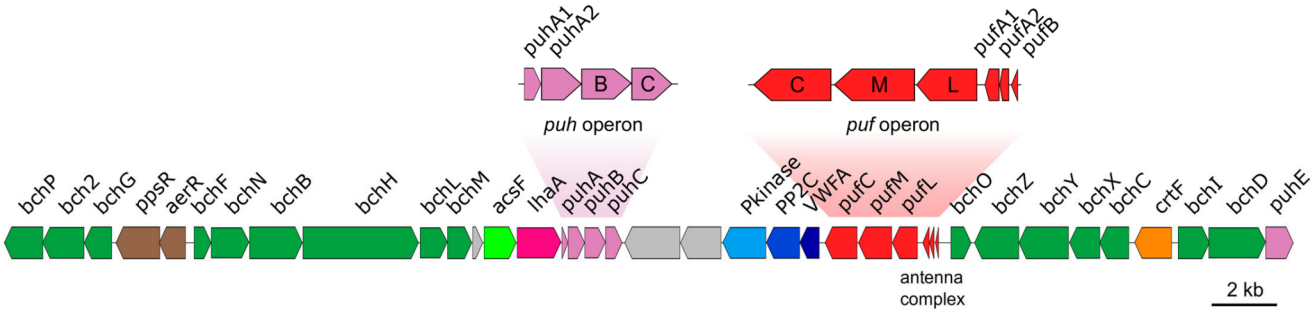

Fig. S1 | Organization of PGC in *Gem. phototrophica*. The *puf* operon is marked in red and the *puh* operon in pink. Genes involved in bacteriochlorophyll synthesis are marked in dark green (*bch* genes) and light green (*acsF*). *CrtF* is marked in orange. Note the presence of two *puhA* genes encoding the Ht and Hc subunits, and two *pufA* genes encoding two forms of the alpha subunit of the antenna complex, in the detailed schemes above.

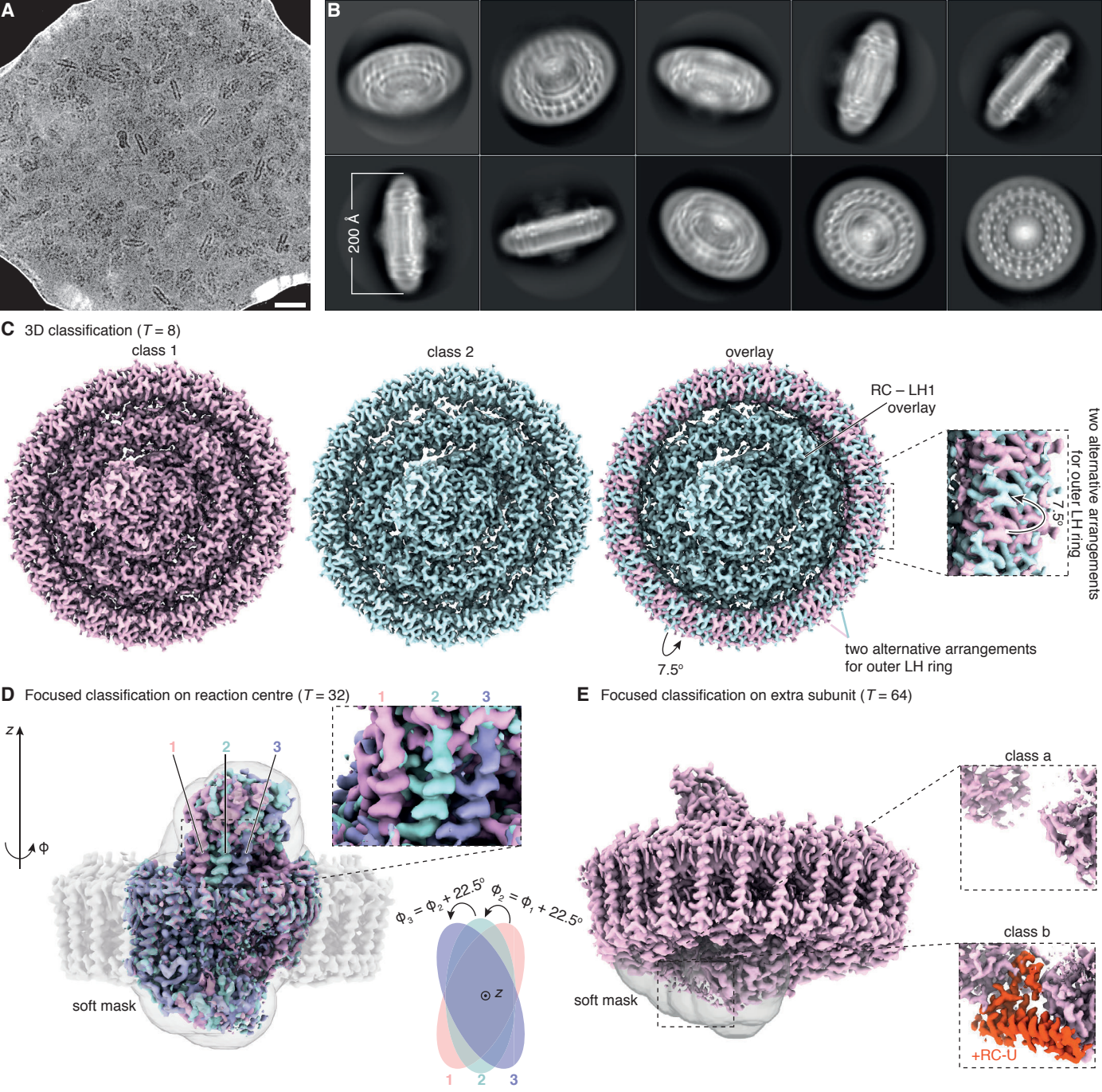
A
B
200 Å
C 3D classification (T = 8)
class 1
class 2
overlay
RC – LH1
overlay
two alternative arrangements
for outer LH ring
7.5°
7.5°
two alternative arrangements
for outer LH ring
D Focused classification on reaction centre (T = 32)
1 2 3
z
Φ
1 2 3
soft mask
Φ3 = Φ2 + 22.5°
Φ2 = Φ1 + 22.5°
z
1 2 3
E Focused classification on extra subunit (T = 64)
class a
class b
soft mask
+RC-U

Fig. S2 | Electron cryomicroscopy of the RC-dLH complex from *G. phototrophica* on HexAuFoil specimen supports. **A**, A representative micrograph of RC-dLH in vitreous ice in the 300 nm hole of a HexAuFoil grid at 2 μm defocus. The micrograph is low-pass filtered to 9 Å and the contrast is adjusted to improve the visibility of the particles. **B**, These selected masked 2D class averages were used for the 3D reconstructions. The diameter of the particles, including the detergent belt, is 200 Å. **C**, Three dimensional classification of the RC-dLH particles revealed two modes of assembly of the outer LHh ring relative to the core RC-LH1 sub-complex. In the two classes (*pink* and *cyan*) the subunits of the outer LHh ring are related by a 7.5° (half of an asymmetric unit) rotation, as shown by the overlay where the two classes are aligned on the RC-LH1 sub-complex. **D**, Further focused three dimensional classification of discarded RC-dLH particles, which resulted in a reconstruction with weak RC density, revealed that the particles were misaligned due to the pseudo-symmetry of the complex. The classification was performed with a soft mask (*gray*) around the RC, and resulted in three classes (*pink*, *cyan*, and *purple*), which are related to each other by a 22.5° rotation of the RC around the pseudo-symmetry axis of the complex. The *inset* shows the density for the same helix in RC in these three classes, demonstrating the misalignment. The schematic shows the relative orientation of the three classes, viewed down the pseudo symmetry (*z*) axis of the complex. Classes 1 and 3 are related by a 45° rotation, which is exactly the angle subtended by one asymmetric unit of the LH1-LHh complex; thus they are equivalent. The particles in these two classes were combined after manually applying -45° rotation around the *z* axis to all particles in class 3. **E**, Further focused three dimensional classification was performed on each class with a mask around a weak density apparent on the cytoplasmic side of the RC. This revealed the presence of a non-obligatory subunit in some of the complexes, later identified as RC-U (*red*).
The *insets* show the density around the RC-U subunit position in the two classes after focused classification. This procedure was performed for both classes 1 and 2 from panel **C**, yielding a total of four classes (two alternative arrangements of LHh, each +/- RC-U).

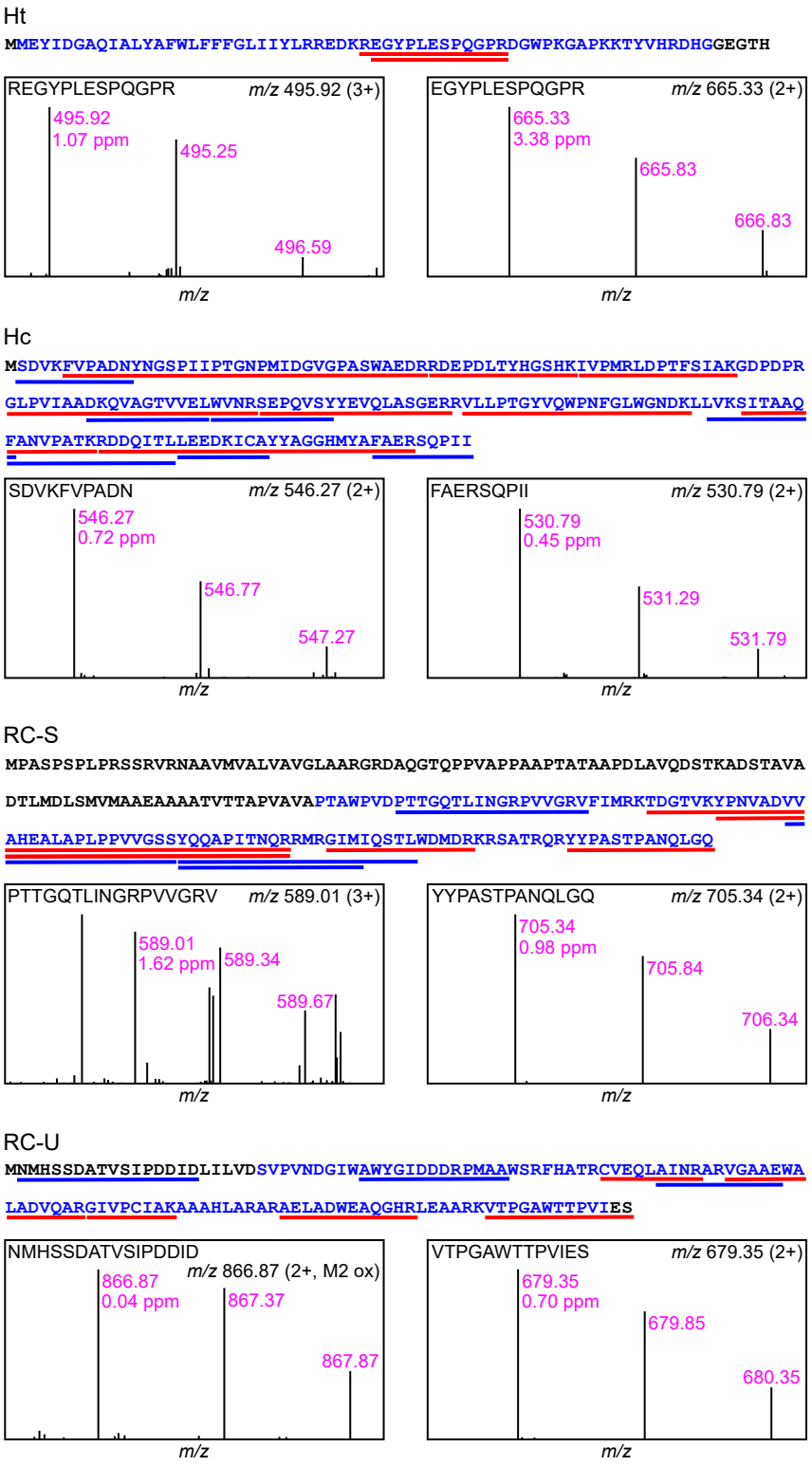

Fig. S3 | Identification of protein subunits Ht (*puhA1* gene product), Hc (*puhA2* gene product), RC-S and RC-U in isolated RC-dLH complexes by mass spectrometry. Sequence coverage by proteolytic peptides generated by endoproteinase Lys-C/trypsin combined and pepsin are indicated by red and blue lines respectively. Amino acids fitted into the cryo-EM map are colored blue. The panels show peptide isotopomer series ions (labelled in magenta) acquired in centroid mode full-MS scans. The peptides are identified by sequence and monoisotopic ion *m*/**z** with mass accuracy expressed in parts per million (ppm). Only peptides at or closest to the protein N- and C-termini are shown as examples in the left and right panels respectively.

```
Gem. phototrophica        -----MMEYIDGAQIALYAFWLFFFG-LIIYLRREDKREGYPLE-SPQ-----GPRDGWP
Blastochloris viridis     MYHGALAQHLDIAQLVWYAQWLVIWTVVLLYLRREDRREGYPLV-EPLGLVKLAPEDGQV
Thermochromatium tepidum  -----ITHYIDAAQITIWAFWLFFFG-LIIYLRREDKREGYPLD-SNRTERSGGRVKVVG
Rhodospirillum rubrum     MNKGDITGYMDVAQVVLYAFWIFFAG-LIIYLRREDRREGYPLE-DAISGKINSLQGLGS
Rps. palustris            MQP---GAYLDLAQVTLYVFWIFFAG-LIFYLRREDKREGYPLY-SDTGGGRLKQ---IG
Rhodobacter sphaeroides   MVGVTAFGNFDLASLAIYSFWIFLAG-LIYYLQTENMREGYPLENEDGTPAANQ-----G

Gem. phototrophica        K-GAPKKTYVHRDHG-GEGTH------MSDVK---FVPADNYNGSPIIPTGNPMIDGVGP
Blastochloris viridis     Y-ELPYPKTFVLPHG-GTVTVPRRRPETRELK---LAQTDGFEGAPLQPTGNPLVDAVGP
Thermochromatium tepidum  FPDLPDPKTFVLPHN-GGTVVAPRVEAPVAVN---ATPFSPAPGSPLVPNGDPMLSGFGP
Rhodospirillum rubrum     VFSIARPKIFKLKTG-ATYAAPNFKRDAVAIK---ATRTAPTAGAPFEPTGNPMTDAVGP
Rps. palustris            IPNPPDPKTYLLRGG-ATRTVPNASNDRPN---VALAPVAPWPGAAFAPTGDPFADGVGP
Rhodobacter sphaeroides   PFPLPKPKTFILPHGRGTLTVPGPESEDR---PIALARTAVSEGFPHAPTGDPMKDGVGP

Gem. phototrophica        ASWAEDRRDEPDLTYHGSHKIVPMRLDPTFSIAKGDPDPRGLPVIAADKQVAGTVVELWV
Blastochloris viridis     ASYAE-RAEVVDATVDGKAKIVPLRVATDFSIAEGDVDPRGLPVVAADGVEAGTVTDLWV
Thermochromatium tepidum  AACPD-RPKHCDLTFEGLPKIVPMRVAKEFSIAEGDPDPRGMTVVGLDGEVAGTVSDVWV
Rhodospirillum rubrum     AAYAL-RDELPDLTLGGQPAIVPLRVAPTFSVAAEDTDPRGLPVVDRKGAVAGKVTDLWI
Rps. palustris            GSYAQ-RQDVPELTLDNLPVIAPLRAAKGMFLDHRDPNPVGMAVVGCDGQVGGTVTEVWV
Rhodobacter sphaeroides   ASWVA-RRDLPELDGHGHNKIKPMKAAAGFHVSAG-KNPIGLPVRGCDLEIAGKVVDIWV

Gem. phototrophica        NRSEPQVSYYEVQLASG--ERRVLLPTGYVQWPNFGLWGNDKLLVKSITAAQFANVPATK
Blastochloris viridis     DRSEHYFRYLELSVAGS--ARTALIPLGFCDVK------KDKIVVTSILSDQFANVPRLQ
Thermochromatium tepidum  DRSEPQIRYLEVEVAAN--KKKVLLPIGFSRFDK----KARKVKVDAIKAAHFANVPTLS
Rhodospirillum rubrum     DRASIAIRYLEVELAATP-GRKVLLPFAATRINAKT--KSKTVTVQSILARHFANVPTIA
Rps. palustris            DRAEVLARYLEVEVAKT-KKR-VLLPVPFALINSPS----GKVSVDAIRGDQFAGVPTTA
Rhodobacter sphaeroides   DIPEQMARFLEVELKDGS---TRLLPMQMVKVQSN------RVHVNALSSDLFAGIPTIK

Gem. phototrophica        RDDQITLLEEDKICAYYAGGHMYAFAERSQPII-------
Blastochloris viridis     SRDQITLREEDKVSAYYAGGLLYATPERAEALL-------
Thermochromatium tepidum  NPDQVTLYEEDKVCAYYAGGKLYATAERAGPLL-------
Rhodospirillum rubrum     KTDSITRREEDKVMAYYSSGYLYS--DRV-----------
Rps. palustris            KPDQVTKLEEDKICAYYGAGTLYATPLRQEPIV-------
Rhodobacter sphaeroides   SPTEVTLLEEDKICGYVAGGLMYAAPKRKSVVAAMLAEYA
```

Fig. S4 | Multiple amino acid sequence alignment of H subunits. Joined *puhA*1 and *puhA*2 genes from *Gem. phototrophica* were aligned along *puhA* sequences from selected phototrophic Proteobacteria. Please note the 6 amino acids missing in *Gem. phototrophica* highlighted in yellow.

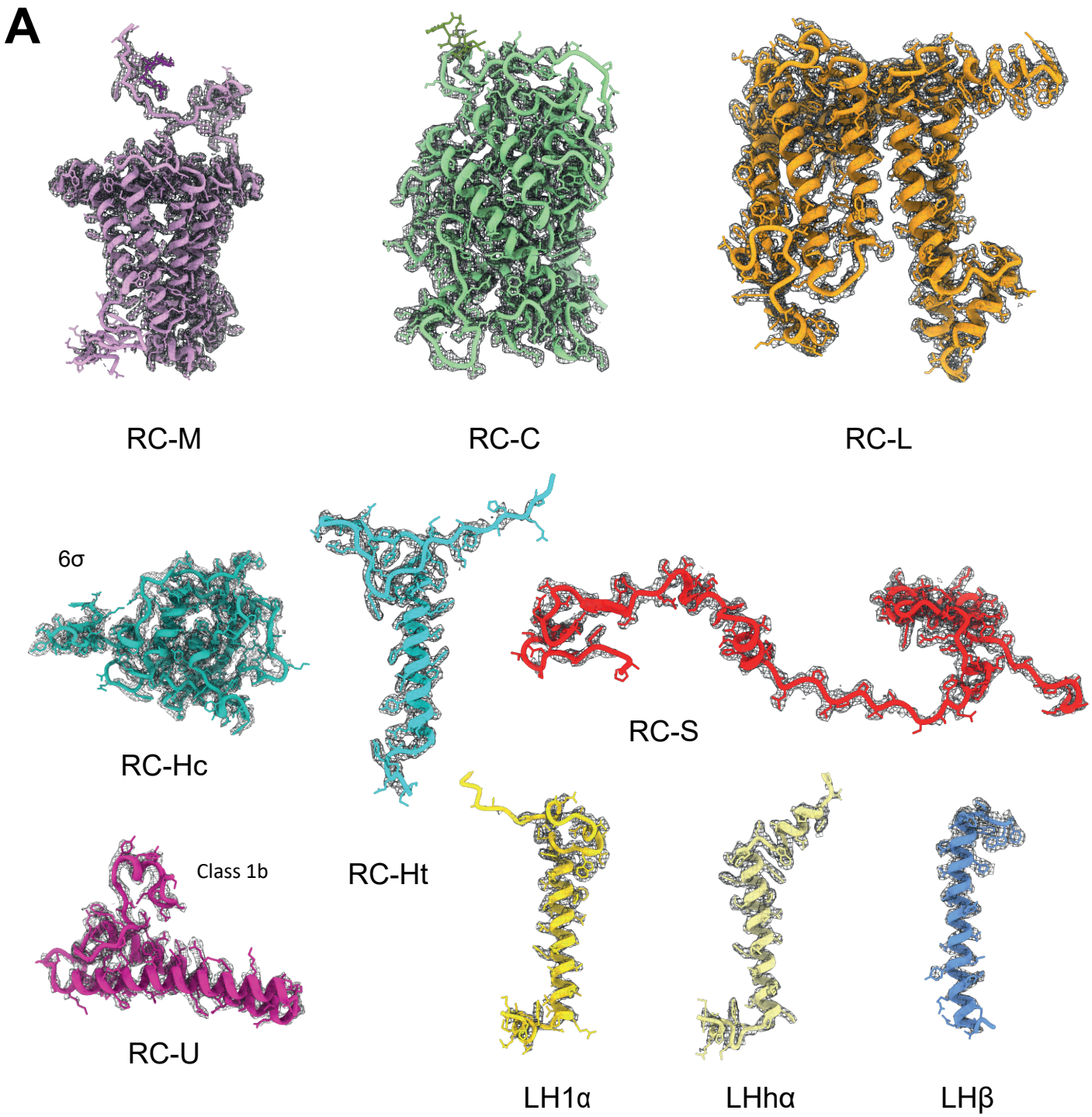
A
RC-M
RC-C
RC-L
6σ
RC-Hc
RC-Ht
RC-S
Class 1b
RC-U
LH1α
LHhα
LHβ
B
i
ii

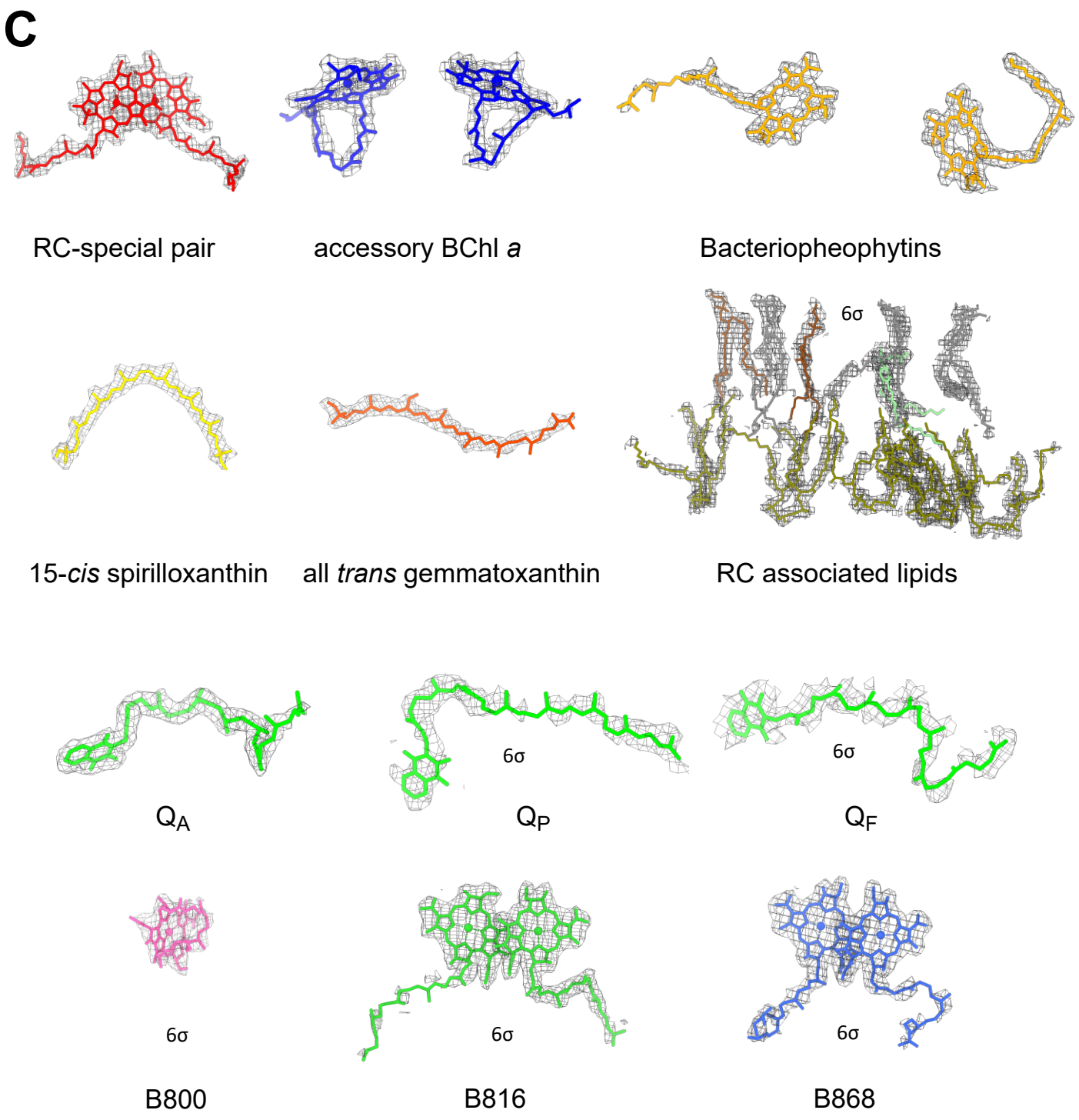

Fig. S5 | Cryo-EM structures of individual polypeptides and co-factors in the *Gem. phototrophica* LH1–RC complex. The color code is the same as in Fig. 1. The density maps represent 8σ contour level unless stated otherwise. **A**, Density maps with fitted models of protein subunits, **B**, *De novo* identification of RC-U. (i) Sidechains were manually assigned and settled in an ISOLDE session, considering both fit to density and physical interactions. (ii) Final model (brown) overlaid with the approximate sequence (white). Matching residues are green; similar polar residues are cyan and similar non-polar residues are yellow. **C**, Density maps with fitted pigments, lipids or quinones.

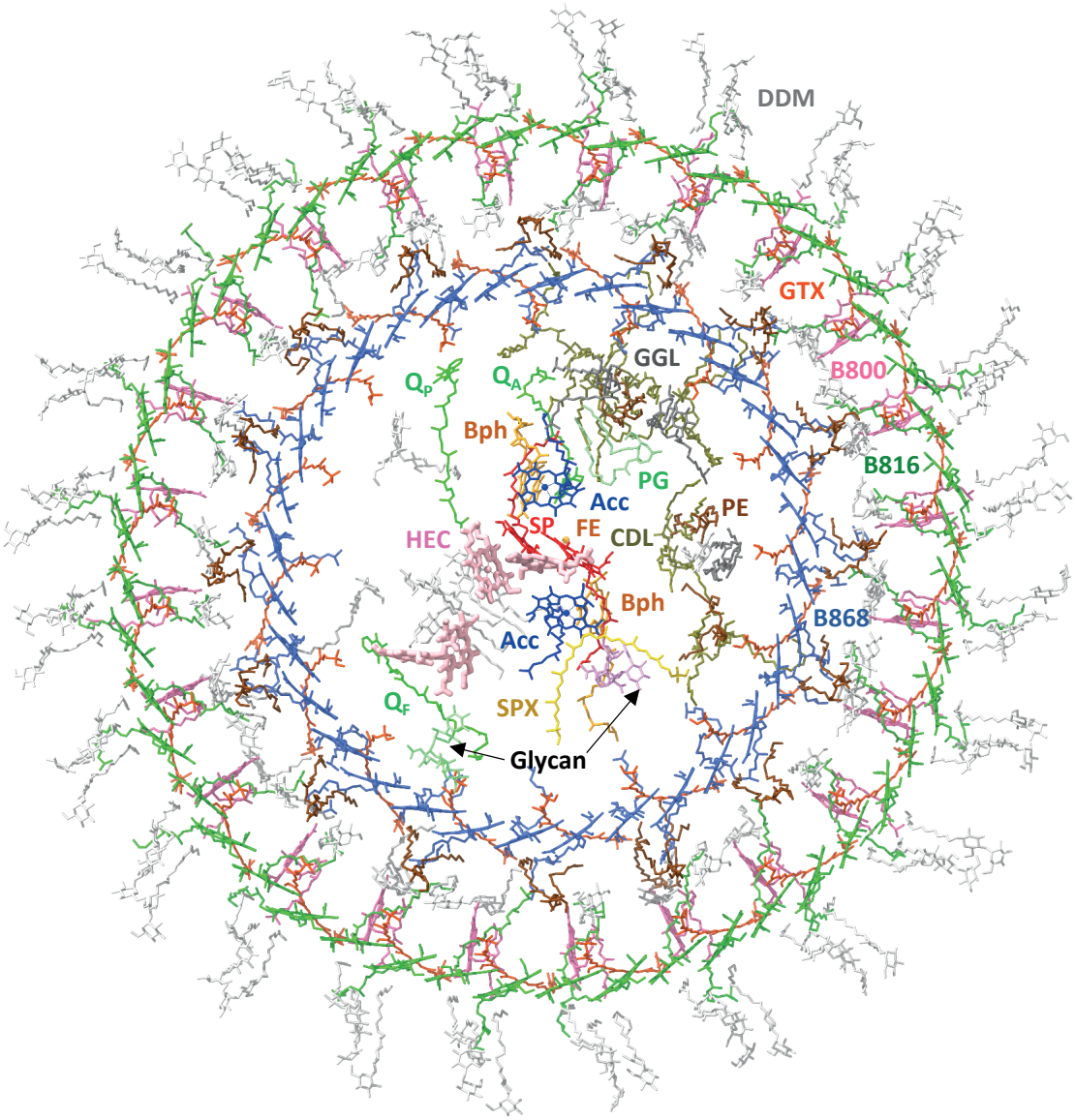

B800	Bacteriochlorophyll *a*	24
B816	Bacteriochlorophyll *a*	48
B868	Bacteriochlorophyll *a*	32
SP	Bacteriochlorophyll *a* (special pair)	2
Acc	Bacteriochlorophyll *a* (accessory pair)	2
	Bacteriochlorophyll *a* (total)	108
Bph	Bacteriopheophytin *a*	2

GTX	Gemmatoxanthin	40
SPX	Spirilloxanthin	1
HEC	Heme C	4
FE	Fe^{2+}	1
PE	Phosphatidyl ethanolamine	20
CDL	Cardiolipin	6
PG	Phosphatidyl glycerol	1
GGL	Glyceroglycolipid	3
DDM	β-dodecylmaltoside	123

MAN*	α-D-mannose	2
RAM*	α-L-rhamnose	2
GUX*	1,2-O-acetyl-α-D-glucuronic acid	2
NDG*	*N*-acetyl-α-D-glucosamine	2
HOH**	water	406

* Labelled as "Glycan"
** Not shown. Numbers vary between maps

Fig. S6 | Co-factor map of the RC-dLH complex The numbers of the different molecules are shown in parentheses. For clarity, water molecules are not shown.

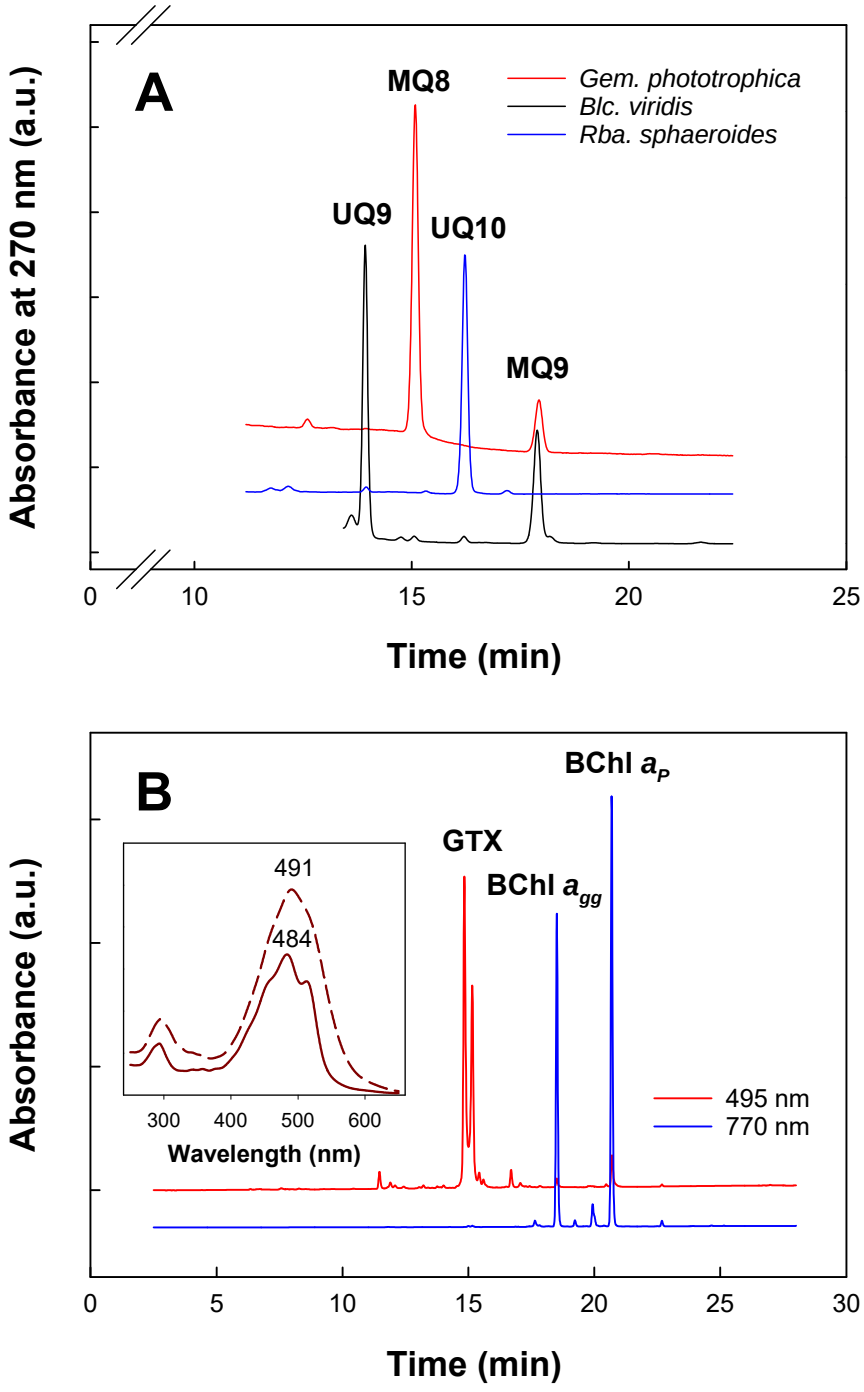

Fig. S7 | Carotenoid and quinone analysis from purified PS complexes. A, Quinone composition of the *Gem. phototrophica* complexes (in red). Composition of *Blastochloris viridis* and *Rhodobacter sphaeroides* complexes are shown for comparison. MQ - menaquinone, UQ - ubiquinone. **B**, HPLC profile of extracted pigments. The complex contains BChl *a* molecules esterified with phytol and geranylgeranyl. In addition there is the main carotenoid gemmatoxanthin (GTX) with two structural isomers. The insert depicts the broad absorption spectrum of gemmatoxanthin in methanol (dashed line), and the more detailed spectrum in hexane (solid line) with three peaks at 455, 484, and 514 nm.

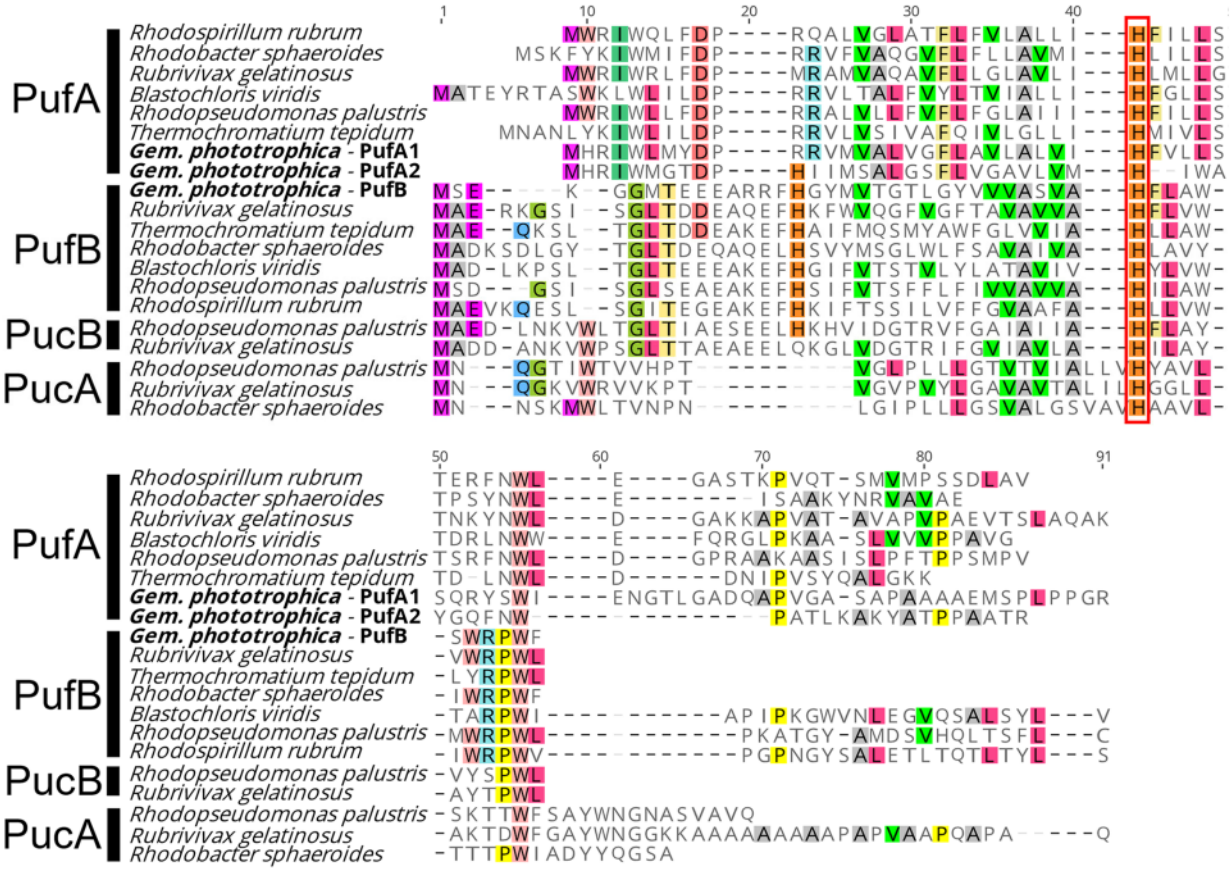

Fig. S8 | Alignment of PufB (locus tag = GEMMAAP_06500), PufA2 (not identified by the NCBI algorithm), and PufA1 (locus tag = GEMMAAP_06495) amino acid sequences of *Gem. phototrophica* and selected phototrophic Proteobacteria. The red box marks the histidines involved in coordinate bond of BChl *a*.

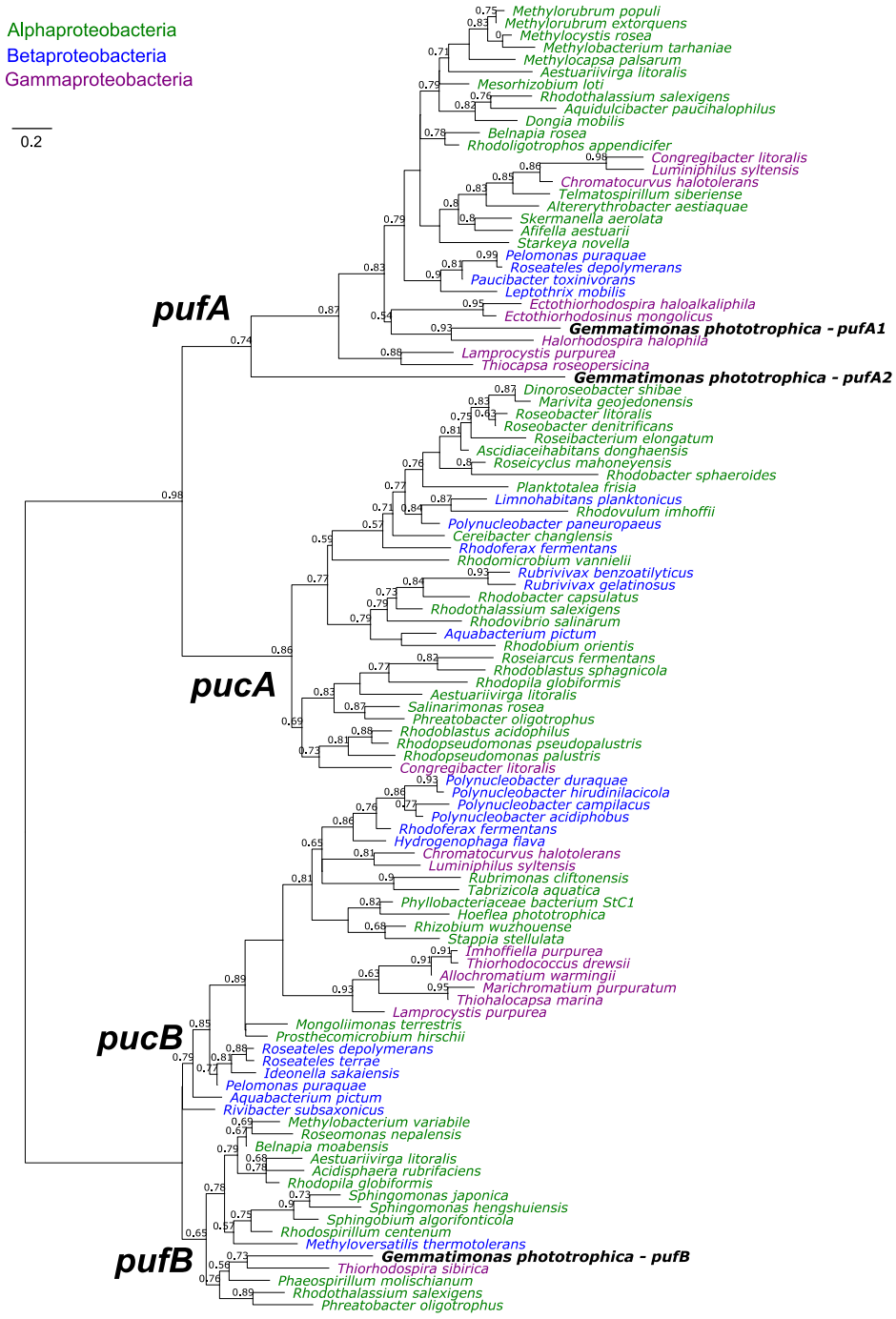

Fig. S9 | Maximum-likelihood tree showing the phylogenetic position of *pufA1*, *pufA2*, and *pufB* genes of *Gem. phototrophica* compared to *pufA*, *pufB*, *pucA*, and *pucB* genes from various phototrophic Proteobacteria. The amino acid sequences were first aligned individually using MUSCLE (ver. 3.8.425) (*46*) with default settings, and then the two alignments were re-aligned using MAFFT (ver. 7.450) (*47*) with initial gap information kept and using the E-INS-i algorithm. Maximum-likelihood unrooted tree was constructed with FastTree2 (*48*) using JTT model and 100 bootstraps. Scale bar represents amino acid substitution rate. Bootstrapping values are shown next to each node. Species are colored according to their taxonomic affiliation.

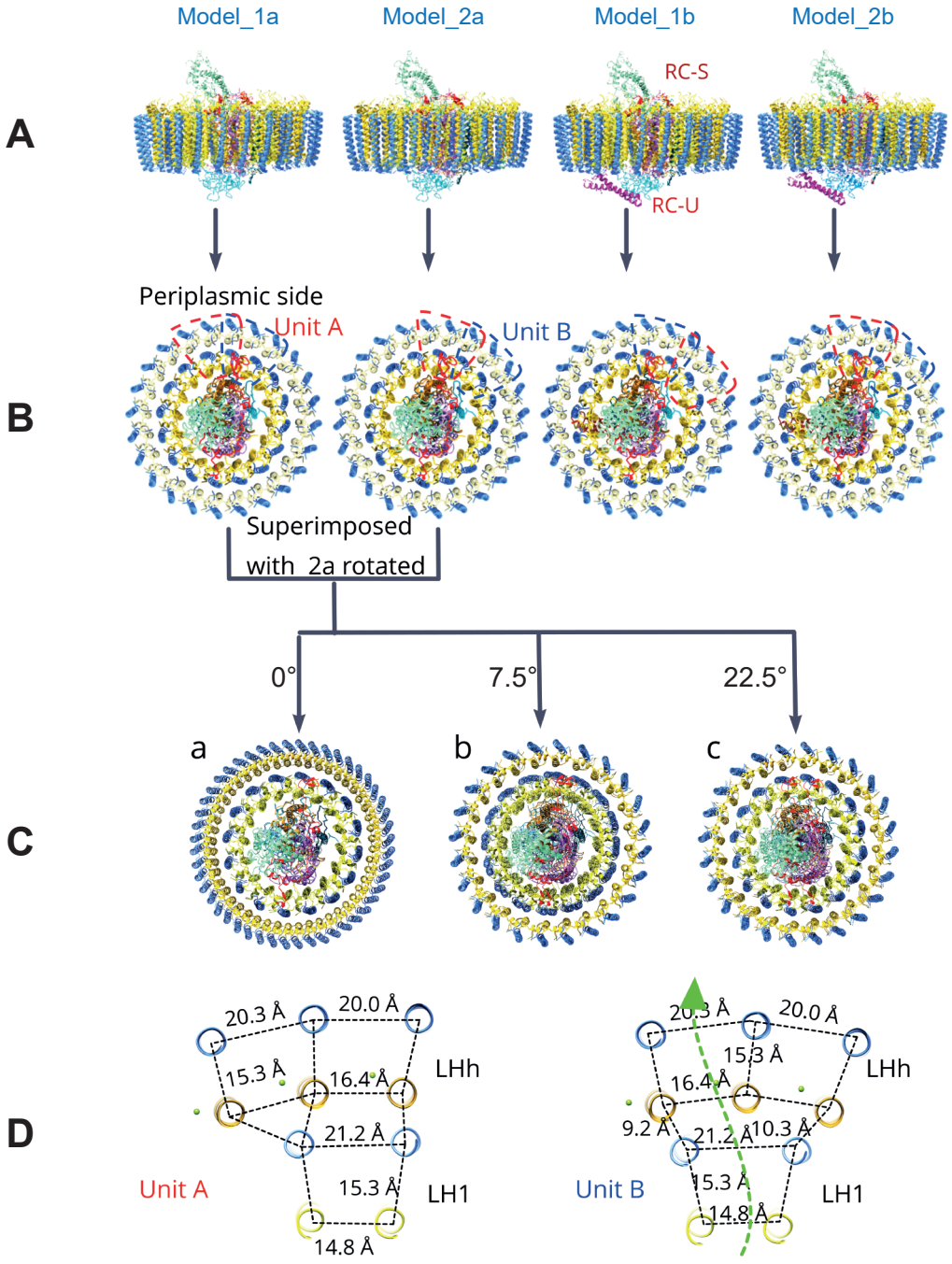

Fig. S10 | Comparison of four different models of the RC-dLH complex. A, Side view of the models. All models have an RC-S polypeptide (red) on the periplasmic side. Models 1a and 2a have no RC-U subunit, but in models 1b and 2b RC-U is attached on the cytoplasmic side. Color coding is the same as that in Fig. 1. **B**, View from periplasmic side. Two different units of the LH ring are classified, unit A (red) and unit B (blue). **C**, Superimposition of model_1a and model_2a with model_2a rotated 0, 7.5 and 22.5 degrees anticlockwise. **C-a**, The RC-LH1 in two models were aligned, but LHh displaced. **C-b**, The model_2a was rotated 7.5 degrees. Only the LHh were aligned, RC-LH1 disordered. **C-c**, the model_2a rotated 22.5 degrees. LHh and LH1 were aligned, but the RCs mixed up. This indicates that the model_1a and model_2a represent two different complexes. The model_1b and model_2b can be done in the same manner. **D**, A slice of unit A and unit B with 0.7 nm thickness centered on the B800 Mg^{2+} ion. Center-to-center distances of transmembrane helices are labeled. A proposed quinone channel is indicated using a green arrow.

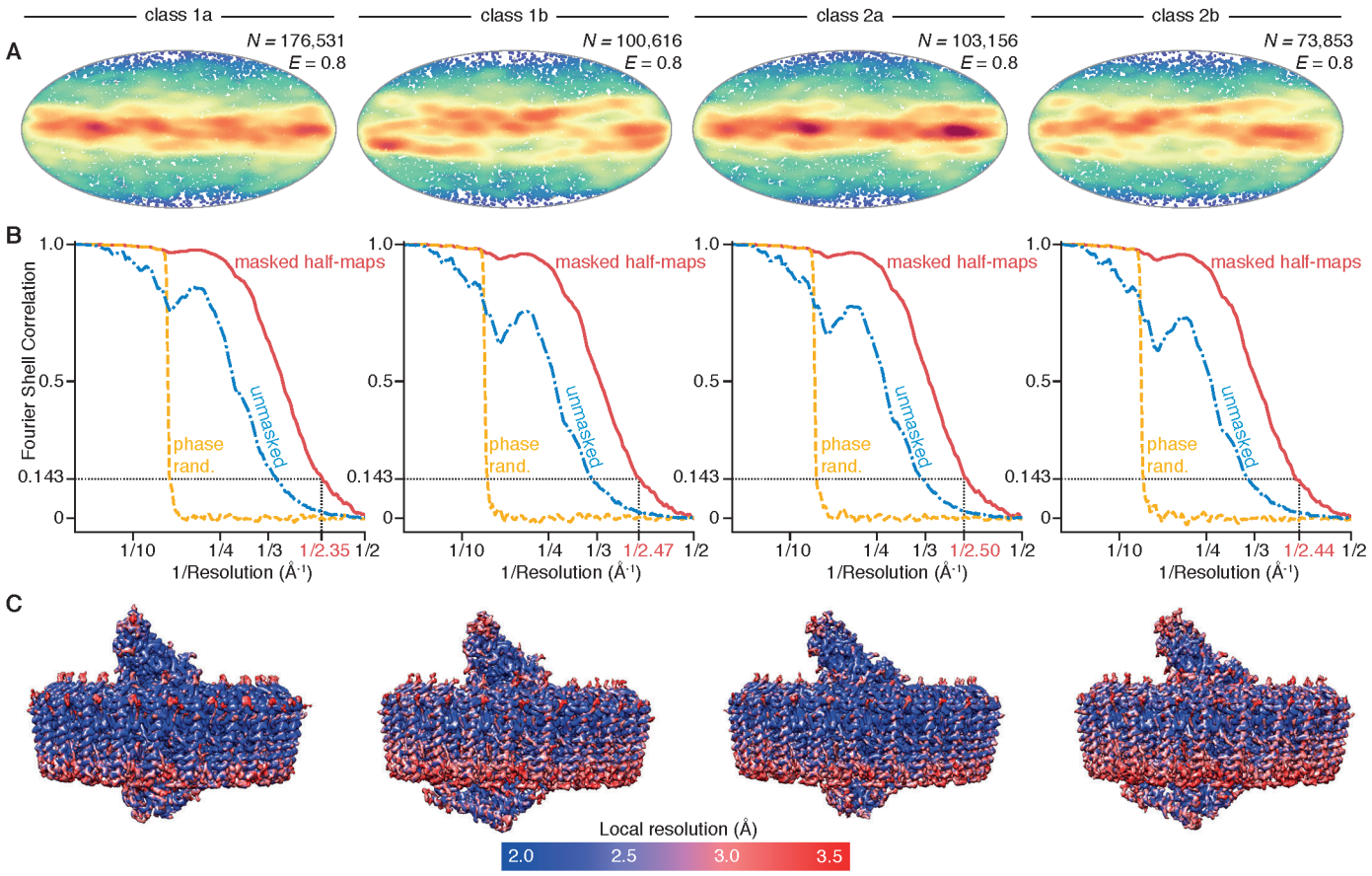

Fig. S11 | Quality of the RC-dLH structures determined by cryo-EM. A, The orientation distribution of the RC-dLH particles in each of the four high-resolution classes, as determined from the 3D refinement, is shown on a Mollweide projection. The meridional axis of the orientation plot is aligned with the pseudosymmetry axis of the LH1 ring. Every point indicates a particle orientation, and the colour scale corresponds to the probability distribution function of the orientations, ranging from 0 (*blue*) to 7 × 10^{-5} (*red*). The efficiency (*39*) E of the orientation distribution is 0.8 for each of the classes, indicating nearly uniform Fourier space coverage. The number of particles N in each class is shown, but all orientation plots show a random subset of 20,000 particle orientations. **B**, Fourier shell correlation (FSC) curves of the masked (*red solid line*), unmasked (*blue dash-dotted line*), and phase randomized (*yellow dashed line*) half maps are shown for each of the four RC-dLH reconstructions. **C**, The maps of the four structures are colored by local resolution, calculated in ResMap (*49*).

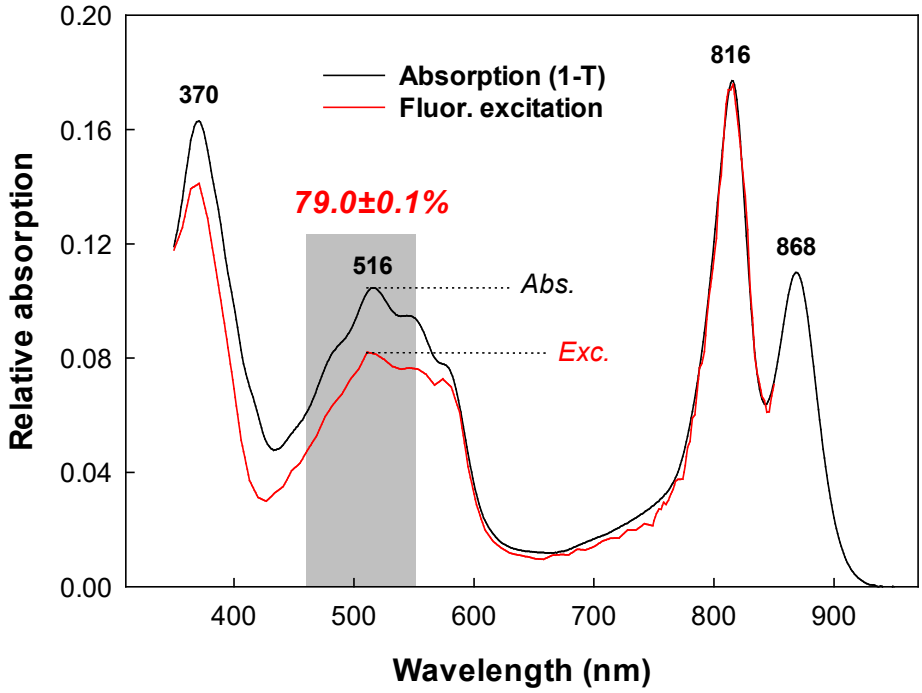

Fig. S12 | Absorption and fluorescence excitation spectra of the RC-dLH complex from *Gem. phototrophica*. The excitation spectrum was measured using a Horiba Fluorolog 3.2.2. instrument in a 1 × 1 cm quartz cuvette with perpendicular geometry. Detection was set at 880 nm. The spectral bandwidth for excitation was set to 6 nm. The spectrum is corrected for spectral dependence of the excitation intensity. The ratios of excitation intensity divided by absorption (*Exc./Abs.*) were calculated for every wavelength between 460 to 550 nm. Then, the average carotenoid-bacteriochlorophyll energy transfer efficiency (in red italics) was calculated as a mean±st.err. from these individual ratios.

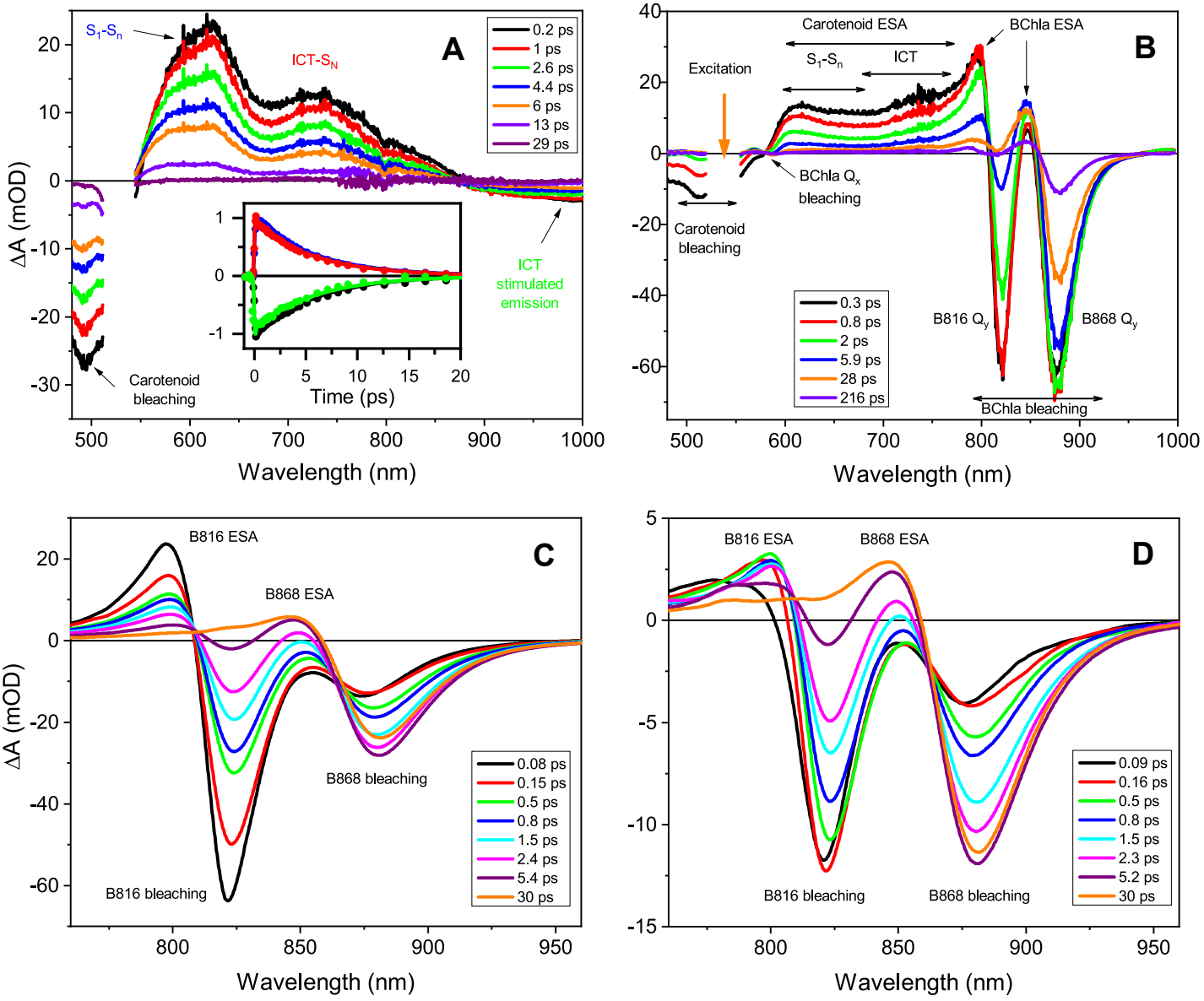
A
S1-Sn
ICT-SN
0.2 ps
1 ps
2.6 ps
4.4 ps
6 ps
13 ps
29 ps
ICT stimulated emission
Carotenoid bleaching
Time (ps)
ΔA (mOD)
Wavelength (nm)
B
Carotenoid ESA
BChla ESA
S1-Sn
ICT
Excitation
BChla Qx bleaching
Carotenoid bleaching
0.3 ps
0.8 ps
2 ps
5.9 ps
28 ps
216 ps
B816 Qy
B868 Qy
BChla bleaching
Wavelength (nm)
C
B816 ESA
B868 ESA
B868 bleaching
B816 bleaching
0.08 ps
0.15 ps
0.5 ps
0.8 ps
1.5 ps
2.4 ps
5.4 ps
30 ps
ΔA (mOD)
Wavelength (nm)
D
B816 ESA
B868 ESA
B816 bleaching
B868 bleaching
0.09 ps
0.16 ps
0.5 ps
0.8 ps
1.5 ps
2.3 ps
5.2 ps
30 ps
Wavelength (nm)

Fig. S13 | Femtosecond transient absorption spectra. **A**, Transient absorption data measured for the isolated carotenoid gemmatoxanthin in methanol. The first spectrum measured at 0.2 ps after excitation at 525 nm has a shape characteristic of the lowest excited state, demonstrating very fast relaxation of the initially excited S_2 state. The presence of an excited state absorption band at 750 nm and negative stimulated emission signal peaking around 1000 nm are a clear sign of intramolecular charge transfer (ICT) state (*50*), in agreement with the recently reported gemmatoxanthin structure featuring a conjugated aldehyde group (*18*). The inset shows kinetics measured at four characteristic wavelengths corresponding to the carotenoid bleaching (black); S_1-S_n transition (blue), ICT-S_N transition (red) and ICT stimulated emission (green). Identical decay properties of these transitions imply the S_1/ICT coupling typical for the carotenoids with conjugated keto group (*51*). **B**, Transient absorption spectra of the RC-dLH complex at a few different delays after excitation of carotenoid at 540 nm. The individual transitions that contribute to the transient absorption spectrum are denoted by arrows. ESA – excited state absorption. ICT – intramolecular charge transfer state. The B816 band is already fully developed 0.3 ps after carotenoid excitation, proving that there is ultrafast energy transfer directly from the carotenoid S_2 state. The B868 bleaching band has also significant magnitude at 0.3 ps, implying that the S_2 route is dominant in both LH1 and LHh rings, but further rise of the band is observed from 0.3 to 0.8 ps. Two processes contribute to this rise; the first is an active S_1/ICT route in LH1 evidenced by shortening of the S_1/ICT lifetime upon binding (see Fig. 7E), the second is LHh-LH1 energy transfer proved by direct excitation of B816 band (see Fig. 7F). **C**, **D**, Direct excitation of B816 and B800, respectively. When the B816 band is excited at 820 nm, the initial spectrum at ~100 fs features B816 ESA at 800 nm and bleaching around 820 nm. These two features decay to form the B868 bleaching band at 880 nm. The latest spectrum at 30 ps, consisting of fully developed bleaching at 880 nm and ESA at ~850 nm, reflects the situation when all excitons are transferred to B868. Note that even at 100 fs there is a substantial signal from B868 due to excitation of the upper exciton band of strongly coupled B868 BChl *a* (*52*). The excitation of B816 induces only B816 to B868 energy transfer as evidenced by the isosbestic point at 808 nm, signalling that no other dynamic processes except the B816 decay are present. When B800 BChl *a* is excited at 785 nm (**D**), the dynamic picture is different. Even at 785 nm some B868 is excited directly via the upper excitonic state, but the zero-crossing point between the B816 ESA and bleaching bands now shifts to the red with time, reflecting additional dynamic process associated with B800 to B816 energy transfer. Since the B800 absorption band is much weaker than B816 (see Fig. 6A), and it overlaps with the B816 ESA, the B800 bleaching is not directly visible in transient absorption spectra, but its presence is inferred from the red shift of the zero-crossing point. The dynamics associated with B800 to B816 energy transfer are apparent for example from the rise component of the B816 ESA band (Fig. 7D). Global fitting the data revealed a 0.4 ps time constant that is present exclusively after 785 nm excitation and 15 reflects B800 to B816 energy transfer.

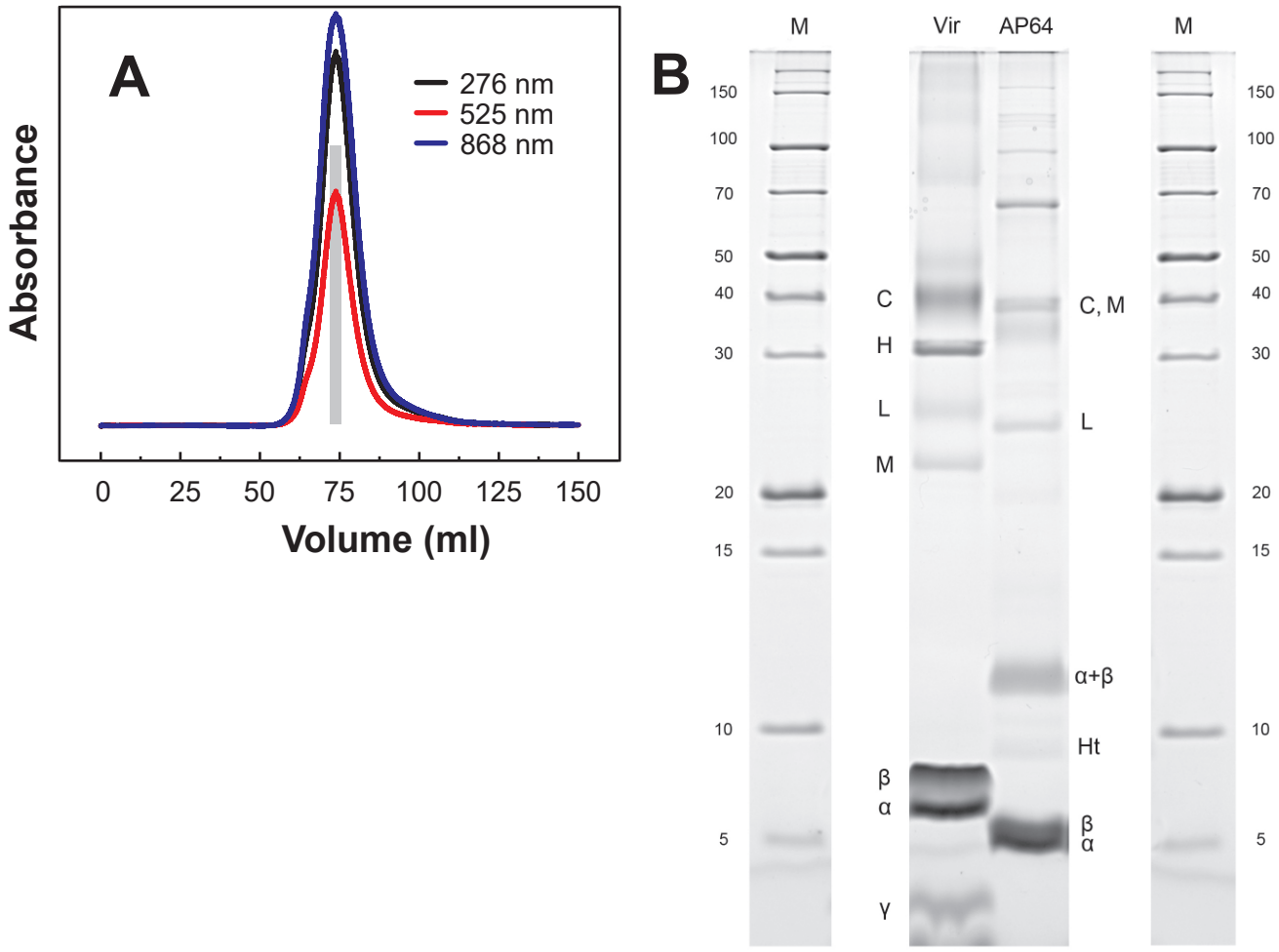

Fig. S14 | Purification of the RC-dLH complex. A, Elution profile from a Superdex S-300 gel filtration column, with the relevant wavelengths are given in the legend. The peak fractions were assayed and shaded grey area represents those (5 x 1 ml) that were selected. The pooled sample was concentrated and sent for cryo-EM analyses. **B**, A 16 to 20 % polyacrylamide gel electrophoresis (*53*) of the RC-dLH complex. The RC-LH1 complex from *Blc. viridis* is shown for comparision. The samples were incubated 10 minutes at 95°C in SDS loading buffer prior to loading. AP64 = RC-dLH complex from *G. phototrophica*, Vir = *Blc. viridis,* M = molecular markers. α+β indicates a band containing undissociated dimers LH1αβ and LHhαβ. The upper bands are incompletely solubilised aggregates of the RC-dLH polypeptides. Due to the extreme structural strength of the complex, the gel is a necessary compromise between harsh denaturation conditions and avoiding degradation of the lower bands.

Table S1: CryoEM data acquisition, model refinement and validation statistics.

Protein source	Photosynthetic bacterium
Data collection and processing	
Microscope	ThermoFisher Titan Krios G3i
Voltage (kV)	300
Camera	Falcon 4
Energy filter	No
Energy filter slit width	N/A
Magnification	120,000×
Defocus range (μm)	-0.8 to -2.4
Mean defoucs (μm)	-1.6
Pixel size (Å)	0.649
Electron flux (e^-/ Å^2/s)	4.48
Electron fluence (e^-/ Å^2)	24.8
Exposure time (sec/frame)	0.29
Electron fluence per frame (e/ Å^2/frame)	1.24
Number of frames per movie	20
Number of movies acquired	19,865
Number of movies used	19,370
Initial no. particle images	1,517,482
Model label	1a / 2a / 1b / 2b
Final no. particle images	176,531 / 103,156 / 100.616 / 73.853
Map resolution (Å, FSC=0.143)	2.35 / 2.50 / 2.47 / 2.44
Symmetry imposed	C1
Specimen temperature	~80K
Particle box size	(400 px)^2 at 0.999 Å/px
Refinement and validation	
Refinement package	COOT, PHENIX, ISOLDE
Initial model	1LGH, 6ET5, 5Y5S
Model resolution (Å, FSC=0.5)	2.6 / 2.8 / 2.8 / 2.8
Map sharpening B factor (Å^2)	-30 / -30 / -30 / -30
Model composition	
Non-hydrogen atoms	55,828 / 55,544 / 56,542 / 56,516
Protein residues	5,052 / 5,023 / 5,149 / 5,151
Molecular weight (kD)	789.89 / 785.79 / 799.61 / 799.65
Protein B factor (Å^2)	46.9 / 49.8 / 51.1 / 48.1
RMS deviations	
Bond length (Å)	0.004 / 0.004 / 0.005 / 0.004
Bond angle (^{0})	1.00 / 1.00 / 1.01 / 0.98
Validation	
MolProbity	0.96 / 0.97 / 0.96 / 0.94
Clashscore	1.93 / 2.02 / 1.96 / 1.83
Poor rotamers (%)	0.41 / 0.31 / 0.28 / 0.22
EMRinger score	5.55 / 5.39 / 5.33 / 5.53
Cβ outliers (>0.25 Å deviation)	0.00 / 0.00 / 0.00 / 0.00
CaBLAM outliers (%)	0.7 / 0.6 / 0.6 / 0.6
Ramachandran plot	
Favoured (%)	98.78 / 98.77 / 98.62 / 98.48
Allowed (%)	1.20 / 1.23 / 1.36 / 1.50
Disallowed (%)	0.02 / 0.00 / 0.02 / 0.02
Ramachandran Z-score	1.36 / 1.63 / 1.29 / 1.32
PDB ID	7O0U / 7O0V / 7O0W / 7O0X
EMDB ID	12679 / 12680 / 12681 / 12682

Movie | Supplementary movie displays the 3D tomography of the RC-dLH1 complex from *G. phototrophica.* The individual sections are displayed in the order starting from the cytoplasmic side towards the periplasmic side of the membrane. Color code is the same as used in Fig. 1.

REFERENCES AND NOTES

1. R. E. Blankenship, *Molecular Mechanisms of Photosynthesis* (John Wiley & Sons, ed. 2, 2014), pp. 312.

2. M. F. Hohmann-Marriott, R. E. Blankenship, Evolution of photosynthesis. *Annu. Rev. Plant Biol.* **62**, 515–548 (2011).

3. W. F. Martin, D. A. Bryant, J. T. Beatty, A physiological perspective on the origin and evolution of photosynthesis. *FEMS Microbiol. Rev.* **42**, 205–232 (2018).

4. M. Sener, J. Strumpfer, S. Abhishek, C. N. Hunter, K. Schulten, Overall energy conversion efficiency of a photosynthetic vesicle. *eLife* **5**, e09541 (2016).

5. D. A. Bryant, A. M. Costas, J. A. Maresca, A. G. Chew, C. G. Klatt, M. M. Bateson, L. J. Tallon, J. Hostetler, W. C. Nelson, J. F. Heidelberg, D. M. Ward, Candidatus *Chloracidobacterium thermophilum*: An aerobic phototrophic Acidobacterium. *Science* **317**, 523–526 (2007).

6. Y. Zeng, F.Y. Feng, H. Medová, J. Dean, M. Koblížek, Functional type 2 photosynthetic reaction centers found in the rare bacterial phylum Gemmatimonadetes. *Proc. Natl. Acad. Sci. U.S.A.* **111**, 7795–7800 (2014).

7. I. Mujakić, A.-Ş. Andrei, T. Shabarova, L.K. Fecskeová, M.M. Salcher, K. Piwosz, R. Ghai, M. Koblížek, Common presence of phototrophic *Gemmatimonadota* in temperate freshwater lakes. *mSystems* **6** (2021).

8. G. E. Chen, D. P. Canniffe, S. F. H. Barnett, S. Hollingshead, A. A. Brindley, C. Vasilev, D. A. Bryant, C. N. Hunter, Complete enzyme set for chlorophyll biosynthesis in *Escherichia coli*. *Sci. Adv.* **4**, eaaq1407 (2018).

9. P. Qian, C. A. Siebert, P. Y. Wang, D. P. Canniffe, C. N. Hunter, Cryo-EM structure of the *Blastochloris viridis* LH1–RC complex at 2.9 Å. *Nature* **556**, 203–208 (2018).

10. Y. Xin, Y. Shi, T. Niu, Q. Wang, W. Niu, X. Huang, W. Ding, L. Yang, R. E. Blankenship, X. Xu, F. Sun, Cryo-EM structure of the RC-LH core complex from an early branching photosynthetic prokaryote. *Nat. Commun.* **9**, 1568 (2018).

11. L. J. Yu, M. Suga, Z. Y. Wang-Otomo, J. R. Shen, Structure of photosynthetic LH1–RC supercomplex at 1.9 Å resolution. *Nature* **556**, 209–213 (2018).

12. P. Qian, T. I. Croll, D. J. K. Swainsbury, P. Castro-Hartmann, N. W. Moriarty, K. Sader, C. N. Hunter, Cryo-EM structure of the *Rhodospirillum rubrum* RC–LH1 complex at 2.5 Å. *Biochem. J.* **478**, 3253–3263 (2021).

13. P. Qian, D. J. K. Swainsbury, T. I. Croll, J. H. Salisbury, E. C. Martin, P. J. Jackson, A. Hitchcock, P. Castro-Hartmann, K. Sader, C. N. Hunter, Cryo-EM structure of the *Rhodobacter sphaeroides* RC–LH1 core monomer complex at 2.5 Å. *Biochem. J.* **478**, 3775–3790 (2021).

14. M. Dachev, D. Bína, R. Sobotka, L. Moravcová, Z. Gardian, D. Kaftan, V. Šlouf, M. Fuciman, T. Polívka, M. Koblížek, Unique double concentric ring organization of light harvesting complexes in *Gemmatimonas phototrophica*. *PLOS Biol.* **15**, e2003943 (2017).

15. E. F. Pettersen, T. D. Goddard, C. C. Huang, E. C. Meng, G. S. Couch, T. I. Croll, J. H. Morris, T. E. Ferrin, UCSF ChimeraX: Structure visualization for researchers, educators, and developers. *Protein Sci.* **30**, 70–82 (2021).

16. D. J. K. Swainsbury, P. Qian, P. J. Jackson, K. M. Faries, D. M. Niedzwiedzki, E. C. Martin, D. A. Farmer, L. A. Malone, R. F. Thompson, N. A. Ranson, D. P. Canniffe, M. J. Dickman, D. Holten, Ch. Kirmaier, A. Hitchcock, C. N. Hunter, Structures of *Rhodopseudomonas palustris* RC-LH1 complexes with open or closed quinone channels. *Sci. Adv.* **7**, abe2631 (2021).

17. K. Tani, R. Kanno, Y. Makino, M. Hall, M. Takenouchi, M. Imanishi, L. Yu, J. Overmann, M. T. Madigan, Y. Kimura, A. Mizoguchi, B. M. Humbel, Z. Wang-Otomo, Cryo-EM structure of a Ca^{2+}-bound photosynthetic LH1-RC complex containing multiple αβ-polypeptides. *Nat. Commun.* **11**, 4955 (2020).

18. Nupur, M. Kuzma, J. Hájek, P. Hrouzek, A. T. Gardiner, M. Lukeš, M. Moos, P. Šimek, M. Koblížek, Structure elucidation of the novel carotenoid gemmatoxanthin from the photosynthetic complex of *Gemmatimonas phototrophica* AP64. *Sci. Rep.* **11**, 15964 (2021).

19. A. T. Gardiner, K. Naydenova, P. Castro-Hartmann, T. C. Nguyen-Phan, Ch. J. Russo, K. Sader, C. N. Hunter, R. J. Cogdell, P. Qian, The 2.4 Å cryo-EM structure of a heptameric light-harvesting 2 complex reveals two carotenoid energy transfer pathways. *Sci. Adv.* **8**, abe4650 (2021).

20. G. McDermott, S. M. Prince, A. A. Freer, A. M. Hawthornthwaite-Lawless, M. Z. Papiz, R. J. Cogdell & N. W. Isaacs, Crystal structure of an integral membrane light-harvesting complex from photosynthetic bacteria. *Nature* **374**, 517–521 (1995).

21. J. Koepke, X. C. Hu, C. Muenke, K. Schulten, H. Michel, The crystal structure of the light-harvesting complex II (B800-B850) from *Rhodospirillum molischanum Structure* **4**, 581–597 (1996).

22. S. J. Jamieson, P. Wang, P. Qian, J. Y. Kirkland, M. J. Conroy, C. N. Hunter, P. A. Bullough, Projection structure of the photosynthetic reaction center–antenna complex of *Rhodospirillum rubrum* at 8.5 Å resolution. *EMBO J.* **21**, 3927–3935 (2002).

23. P. Qian, M. Z. Papiz, P. J. Jackson, A. A. Brindley, I. W. Ng, J. D. Olsen, M. J. Dickman, P. A. Bullough, C. N. Hunter, Three-dimensional structure of the *Rhodobacter sphaeroides* RC-LH1-PufX

complex: Dimerization and quinone channels promoted by PufX. *Biochemistry* **52**, 7575–7585 (2013).

24. A. W. Roszak, T. D. Howard, J. Southall, A. T. Gardiner, Ch. J. Law, N. W. Isaacs, R. J. Cogdell, Crystal structure of the RC-LH1 core complex from *Rhodopseudomonas palustris. Science* **302**, 1969–1972 (2003).

25. P. Qian, H. A. Addlesee, A. V. Ruban, P. Wang, P. A. Bullough, C. N. Hunter, A reaction center-light-harvesting 1 complex (RC-LH1) from a *Rhodospirillum rubrum* mutant with altered esterifying pigments: Characterization by optical spectroscopy and cryo-electron microscopy. *J. Biol. Chem.* **278**, 23678–23685 (2003).

26. R. J. Cogdell, A. Gall, J. Köhler, The architecture and function of the light-harvesting apparatus of purple bacteria: From single molecules to in vivo membranes. *Q. Rev. Biophys.* **39**, 227–324 (2006).

27. T. Polivka, H. A. Frank, Molecular factors controlling photosynthetic light harvesting by carotenoids. *Acc. Chem. Res.* **43**, 1125–1134 (2010).

28. S. Hess, M. Chachisvilis, K. Timpmann, M. R. Jones, G. J. Fowler, C. N. Hunter, V. Sundström, Temporally and spectrally resolved subpicosecond energy transfer within the peripheral antenna complex (LH2) and from LH2 to the core antenna complex in photosynthetic purple bacteria. *Proc. Natl. Acad. Sci. U.S.A.* **92**, 12333–12337 (1995).

29. Y. Zeng, Nupur, N. Wu, A. M. Madsen, X. Chen, A. T. Gardiner, M. Koblížek, *Gemmatimonas groenlandica* sp. nov. is an aerobic anoxygenic phototroph in the phylum Gemmatimonadetes. *Front. Microbiol.* **11**, 606612 (2021).

30. K. Naydenova, P. Jia, C. J. Russo, Electron cryomicroscopy with sub-Angstrom specimen movement. *Science*, 223–226 (2020).

31. J. R. Bellare, H. T. David, L. E. Scriven, Y. Talmon, Controlled environment vitrification system: An improved sample preparation technique. *J. Electron Microsc. Tech.* **10**, 87–111 (1988).

32. C. J. Russo, L. A. Passmore, Ultrastable gold substrates: Properties of a support for high-resolution electron cryomicroscopy of biological specimens. *J. Struct. Biol.* **193**, 33–44 (2016).

33. K. Sader, R. Matadeen, P. C. Hartmann, T. Halsan, C. Schlichten, Industrial cryo-EM facility setup and management. *Acta Cryst. D* **76**, 313–325 (2020).

34. J. Zivanov, T. Nakane, B. O. Forsberg, D. Kimanius, W. J. H. Hagen, E. Lindahl, S. H. W. Scheres, New tools for automated high-resolution cryo-EM structure determination in RELION-3. *eLife* **7**, e42166 (2018).

35. A. Rohou, N. Grigorieff, CTFFIND4: Fast and accurate defocus estimation from electron micrographs. *J. Struct. Biol.* **192**, 216–221 (2015).

36. T. Wagner, F. Merino, M. Stabrin, T. Moriya, C. Antoni, A. Apelbaum, P. Hagel, O. Sitsel, T. Raisch, D. Prumbaum, D. Quentin, D. Roderer, S. Tacke, B. Siebolds, E. Schubert, T. R. Shaikh, P. Lill, Ch. Gatsogiannis, S. Raunser, SPHIRE-crYOLO is a fast and accurate fully automated particle picker for cryo-EM. *Commun. Biol.* **2**, 218 (2019).

37. J. Zivanov, T. Nakane, S. H. W. Scheres, A Bayesian approach to beam-induced motion correction in cryo-EM single-particle analysis. *Iucrj* **6**, 5–17 (2019).

38. K. Ramlaul, C. M. Palmer, T. Nakane, C. H. S. Aylett, Mitigating local over-fitting during single particle reconstruction with SIDESPLITTER. *J. Struct. Biol.* **211**, 107545 (2020).

39. K. Naydenova, C. J. Russo, Measuring the effects of particle orientation to improve the efficiency of electron cryomicroscopy. *Nat. Commun.* **8**, 629 (2017).

40. P. Emsley, K. Cowtan, Coot: Model-building tools for molecular graphics. *Acta Crystallogr*. *D* **60**, 2126–2132 (2004).

41. T. I. Croll, ISOLDE: A physically realistic environment for model building into low-resolution electron-density maps. *Acta Crystallogr. D* **74**, 519–530 (2018).

42. D. Shaya, W. Zhao, M. Garron, Z. Xiao, Q. Cui, Z. Zhang, T. Sulea, R. J. Linhardt, M. Cygler, Catalytic mechanism of heparinase II investigated by site-directed mutagenesis and the crystal structure with its substrate. *J. Biol. Chem.* **285**, 20051–20061 (2010).

43. M. Tiemeyer, K. Aoki, J. Paulson, R. D. Cummings, W. S. York, N. G. Karlsson, F. Lisacek, N. H. Packer, M. P. Campbell, N. P. Aoki, A. Fujita, M. Matsubara, D. Shinmachi, S. Tsuchiya, I. Yamada, M. Pierce, R. Ranzinger, H. Narimatsu, K. F. Aoki-Kinoshita, GlyTouCan: An accessible glycan structure repository. *Glycobiology* **27**, 915–919 (2017).

44. V. Lombard, H. G. Ramulu, E. Drula, P. M. Coutinho, B. Henrissat, The Carbohydrate-active enzymes database (CAZy) in 2013. *Nucleic Acids Res.* **42**, D490–D495 (2014).

45. J. Agirre, J. Iglesias-Fernández, C. Rovira, G. J. Davies, K. S. Wilson, K. D. Cowtan, Privateer: Software for the conformational validation of carbohydrate structures. *Nat. Struct. Mol. Boil.* **22**, 833–834 (2015).

46. R. C. Edgar, MUSCLE: Multiple sequence alignment with high accuracy and high throughput. *Nucleic Acids Res*. **32**, 1792–1797 (2004).

47. K. Katoh, D. M. Standley, MAFFT multiple sequence alignment software version 7: Improvements in performance and usability. *Mol. Biol. Evol*. **30**, 772–780 (2013).

48. M. N. Price, P. S. Dehal, A. P. Arkin, FastTree 2–approximately maximum-likelihood trees for large alignments. *PLOS ONE* **5**, e9490 (2010).

49. A. Kucukelbir, F. J. Sigworth, H. D. Tagare, Quantifying the local resolution of cryo-EM density maps. *Nat. Methods* **11**, 63–65 (2014).

50. D. Zigmantas, R. G. Hiller, F. P. Sharples, H. A. Frank, V. Sundströma, T. Polívka, Effect of a conjugated carbonyl group on the photophysical properties of carotenoids. *Phys. Chem. Chem. Phys.* **6**, 3009–3016 (2004).

51. R. G. West, M. Fuciman, H. Staleva-Musto, V. Šebelík, D. Bína, M. Durchan, V. Kuznetsova, T. Polívka, Equilibration dependence of fucoxanthin S1 and ICT signatures on polarity, proticity, and temperature by multipulse femtosecond absorption spectroscopy. *J. Phys. Chem. B* **122**, 7264–7276 (2018).

52. G. D. Scholes, G. R. Fleming, On the mechanism of light harvesting in photosynthetic purple bacteria: B800 to B850 energy transfer. *J. Phys. Chem. B* 104, 1854–1868 (2000).

53. M. Dobáková, R. Sobotka, M. Tichý, J. Komenda, Psb28 protein is involved in the biogenesis of the photosystem II inner antenna CP47 (PsbB) in the cyanobacterium *Synechocystis* sp. PCC 6803. *Plant Physiol.* **149**, 1076–1086 (2009).